

The swinging counterweight trebuchet On scaling and optimization

E Horsdal

Department of Physics and Astronomy, Aarhus University, DK-8000 Aarhus C,
Denmark

E-mail: horsdal@phys.au.dk

Abstract. The swinging counterweight trebuchet was at its full blossom in the Late Middle Ages an artillery piece of great importance that could destroy the defenses of castles under siege by bombardment with stones from considerable distances. The exact dimensions of these engines are unfortunately unknown, but would have been valuable for an assessment of the true significance of the weapon. Presumed dimensions derived from interpreted historical accounts must be tested and examined critically. This has been done by full-scale experimental reconstructions or by *ad hoc* theoretical estimates. A more systematic approach is made possible by the present theory, which is based on a mathematical quality function for the trebuchet. This function can be maximized and the maximizing design parameters are by definition the optimal parameters. A simple analytical expression for these optimal parameters is given.

1. Introduction

Powered by gravity alone, the swinging counterweight trebuchet gradually became the most important artillery piece within the arsenals of several civilizations beginning around the year 1200 or earlier and lasting for more than 200 years into the era of gunpowder weaponry beginning during the late part of the Hundred Years' War [1, 2, 3, 4]. Improvements of the weapon over the period were based entirely on intuition, craftsmanship and trial and error [1], because the physical and mathematical sciences were not sufficiently developed to be of much help. It is interesting nowadays to investigate the full theoretical potential of the weapon by using contemporary methods even though it is difficult to decide how much this unknown potential was unfolded historically.

A trebuchet with hinged counterweight is composed of three pendulums. A single pendulum is a relatively simple dynamical system, but three acting together and not limited to small swings constitute a quite complex problem that is difficult to comprehend, and tuning it for a specific purpose is a difficult task. It is not a good strategy to focus on individual parts, one after the other, because the motion of one part depends intricately on the motion of the two others. Instead, all parameters must be adjusted simultaneously and it requires a complete solution to the dynamical problem.

A discussion of good design presupposes agreement on what it entails, and the formulation must be sufficiently precise that it can be expressed mathematically as a quality function \mathcal{Q} that can be maximized. We suggest that \mathcal{Q} balances the opposing desires for having both a powerful and a light and durable weapon that is easily built, moved and operated. Thus, a trebuchet of good construction must have great destructive potential without resorting to excessive overall size or weight. The function \mathcal{Q} must therefore depend on range relative to size, on projectile mass relative to counterweight mass, on efficiency of transforming energy from potential to kinetic, and on internal reaction forces that wear down the machine. Different functions \mathcal{Q} can be constructed, and any design that maximizes a quality function can be considered optimal, so this property is not unique, but different optimized design turn out to be quite similar, so a clear picture emerges after all.

Capacities of historical trebuchets are most often specified by range and mass of the projectile, which are R and m , respectively [5, 6]. Here, we replace m by the energy T delivered to the target, because the pair R and T is a better starting point for analysis and aligns with contemporary assessment of artillery. Except in a few specific cases, it is also assumed for simplicity that aerodynamic and sliding friction losses can be ignored and that the target is at the same elevation as the base of the engine.

The many adjustable parameters of a trebuchet opens a huge space of conceivable design which is difficult to navigate without guidelines. Craftsmanship and experience from the battlefield drove the historical development and good trebuchets were most likely built in many cases, but early written information to document this is unfortunately sparse and the available pictorial renditions are difficult to interpret. Contemporary studies of sieges, where trebuchets were deployed, are made difficult by this lack of documentation [5, 6]. The desired range R of an artillery piece depends on defense capabilities and local topography, and the desired energy T on building methods and materials. The actual assessment of the necessary capacity (R, T) must be made by experts in military history, but when this is done the dimensions of a weapon, that is optimal according to the principles presented here, follow from only a few simple algebraic calculations.

2. Trebuchet

The basic design and functionality of a trebuchet was described recently from different perspectives by Saimre [7] and Denny [8]. Here, we give only a brief account that refers to the schematic diagram in figure 1a where the necessary variables are identified. The beam, which extends from H to S, is divided into two sections by a pivoting axle P-P seen best in figure 1b. The long section L_1 carries a sling of length L_4 , and a counterweight of mass M is hinged at H to the short section L_2 by an arm of length L_3 . The projectile has mass m and is placed in a pouch with two ropes that constitute the sling. A spigot S at the end of the long beam section is part of a clever release mechanism for the projectile. The center of mass for the beam is at CM and the mass is m_b . The beam is treated

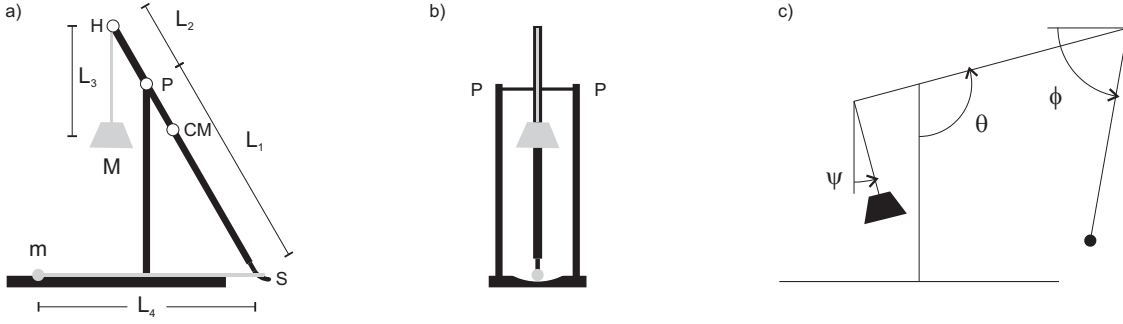


Figure 1. Trebuchet. a) Initial configuration with projectile in trough and target to the left. H: hinge. P: pivot. S: spigot. b) Same, but seen from target. c) Snapshot of movement with generalized angular coordinates.

as a rigid and thin cylinder with diameter D and moment of inertia relative to P given by $\mathcal{I}_b = \frac{1}{3}m_b(L_1^2 - L_1L_2 + L_2^2)$. The distance from P to CM is $L_{CM} = (L_1 - L_2)/2$.

When the trebuchet is fired, gravity pulls M down so beam and sling rotate about the pivot and spigot, respectively. A snapshot of the motion is shown in figure 1c. The projectile has been lifted off the trough and it is released into a ballistic path towards a target to the left at a later time determined by the spigot setting. Figure 1c also identifies three angles, which are the generalized coordinates of the internal movement.

The counterweight and projectile are treated as point particles. The total rotational kinetic energy is then $T_r = \frac{1}{2}\mathcal{I}_b\dot{\theta}^2$, where dot-notation is used for differentiation with respect to time, $\dot{\theta} = d\theta/dt$. The total translational kinetic energy T_t is the sum of the kinetic energies of the three centers of mass. Each has the form $\frac{1}{2}m\dot{\mathbf{r}}^2$, where the velocity $\dot{\mathbf{r}}$ depends on time through the angles (θ, ψ, ϕ) and their derivatives $(\dot{\theta}, \dot{\psi}, \dot{\phi})$. The total kinetic energy of the trebuchet is $T = T_r + T_t$, and the total potential energy U is the sum of the potential energies of the three centers of mass. U depends on time through the angles, but is independent of angular speeds. The kinetic and potential energies determine the equations of motion that govern the internal movement. This has three phases: The projectile slides in the trough during phase I, which lasts as long as the supporting normal force differs from zero. It is lifted and rotates relative to the spigot during phase II, and phase III starts when the projectile is released from the pouch.

The equations for the inner movement determine θ , ψ and ϕ as functions of time for given initial conditions and parameters for the engine. These are, respectively

$$\theta_i, \quad \psi_i, \quad \phi_i, \quad \dot{\theta}_i, \quad \dot{\psi}_i, \quad \text{and} \quad \dot{\phi}_i, \quad (1)$$

and

$$L_1, \quad L_2, \quad L_3, \quad L_4, \quad D, \quad M, \quad m \quad \text{and} \quad m_b. \quad (2)$$

The many variables imply a multitude of machines and this must be reduced. Historical trebuchets were never propped and always at rest prior to a shot, so $\psi_i = \phi_i = 0$ and $\dot{\theta}_i = \dot{\psi}_i = \dot{\phi}_i = 0$. The change of potential energy from a shot is initiated and until the engine has come to rest again is

$$\Delta U = (ML_2 - m_bL_{CM})g(1 + \cos \theta_i), \quad (3)$$

where g is the local gravitational acceleration. The initial beam angle θ_i should be as small as practically possible to maximize ΔU . We have chosen $\theta_i = 30^\circ$ as a reasonable standard.

An engine works best when M falls almost vertically for as long as possible, and this implies a long arm L_3 . The longest is $L_2 + L_3 = H$, where $H = L_1 \cos \theta_i$ is the height of the pivot. A more realistic choice is $L_2 + L_3 = FH$ with $F = 2/3$ or $1/2$. Both values are examined to illustrate how much $F < 1$ impairs the performance.

Seven of the 14 parameters in (1) and (2) are now fixed, and the diameter D is a function of beam mass and length for a given density of the wood used. Six free parameters therefore remain. They are

$$L_1, \quad L_2, \quad L_4, \quad M, \quad m \quad \text{and} \quad m_b . \quad (4)$$

3. Scaling, fewer free parameters and an internal force

The masses and lengths in the equations of motion can be measured such they become dimensionless. We choose to measure masses in units of the counterweight mass M and lengths in units of the short beam section L_2 . The units of time, speed, energy and force are then $(L_2/g)^{1/2}$, $(L_2g)^{1/2}$, MgL_2 and Mg , respectively. The dimensionless form of the coupled differential equations for the internal movement are written explicitly in Appendix A. They include the five parameters

$$l = \frac{L_1}{L_2}, \quad l_4 = \frac{L_4}{L_1}, \quad L = \frac{L_3}{L_2}, \quad \mu_b = \frac{m_b}{M} \quad \text{and} \quad \mu = \frac{m}{M} , \quad (5)$$

but $L = Fl \cos \theta_i - 1$ is not a free parameter, so these are the four

$$l, \quad l_4, \quad \mu_b \quad \text{and} \quad \mu , \quad (6)$$

where the first three are design parameters that refer to the engine as such, and μ relates to the projectile. The efficiency of the engine ϵ and, for the projectile, the scaled range ρ and kinetic energy at target τ_e are

$$\epsilon = \frac{T}{\Delta U}, \quad \rho = \frac{R}{L_2}, \quad \text{and} \quad \tau_e = \frac{T}{MgL_2} , \quad (7)$$

where

$$T = \frac{1}{2}mv_r^2 + mgh_r . \quad (8)$$

Here v_r and h_r are the projectile's speed and height at release, respectively. The efficiency defined in (7) reaches one if the engine can be adjusted such that beam and counterweight are permanently at rest at the end of phase II. Note that efficiency is defined differently in [7, 8].

The equations of motion can be solved only by numerical methods except in special cases. The first instant of the motion is such a case. When the initial values of angles and angular speeds are inserted in (A.1) and (A.2), the equations become algebraic in the angular accelerations $\ddot{\theta}$ and $\ddot{\psi}$ and are easily solved. The initial acceleration of the counterweight \mathbf{a}_{CW} can then be calculated. It points straight down as in a free fall,

but the acceleration is reduced relative to gravity. The total force on the counterweight equals mass times acceleration and is the sum of (downward) gravity $M\mathbf{g}$ and (upward) reaction from the hinge \mathbf{F}_H , *i.e.* $M\mathbf{a}_{CW} = M\mathbf{g} + \mathbf{F}_H$. Therefore, $\mathbf{F}_H = -M\mathbf{g}$ before a shot is initiated ($\mathbf{a}_{CW} = \mathbf{0}$), but immediately after

$$\begin{aligned} F_H &= -M\mathbf{g} \left(1 - \frac{L_2 \sin^2 \theta_i (ML_2 - m_b L_{CM})}{ML_2^2 \sin^2 \theta_i + \mathcal{I}_b + mL_1^2 \cos^2 \theta_i} \right) \\ &= -M\mathbf{g} \left(1 - \frac{\sin^2 \theta_i (1 - \frac{1}{2}\mu_b(l-1))}{\sin^2 \theta_i + \frac{1}{3}\mu_b(l^2 - l + 1) + \mu l^2 \cos^2 \theta_i} \right) \\ &= -M\mathbf{g} (1 - 0.42) \quad \text{with } \theta_i = 45^0, l = 5, \mu_b = 6\% \text{ and } \mu = 1\% . \end{aligned}$$

This exemplifies the calculation of an internal force from the internal movement.

4. Strength of beam and relation between lengths and masses

A good trebuchet transfers most of the counterweight's potential energy to the projectile. Some is used, however, to raise and move the center of mass of the beam, so a light beam is desirable, but the beam must also be sufficiently strong. In preparation for a shot, the counterweight is lifted by the short end of the beam as the long end is being pulled down. The load is strongest when the beam is horizontal, and here it can be considered quasi-static and clamped at the pivot. The bending of the two beam sections are then [9]

$$\beta_1 = \frac{MgL_1L_2}{3\mathcal{M}_e\mathcal{I}} \quad \text{and} \quad \beta_2 = \frac{MgL_2^2}{3\mathcal{M}_e\mathcal{I}} \quad \text{with} \quad \mathcal{I} = \frac{\pi}{64}D^4, \quad (9)$$

where $u_1 = \beta_1L_1$ and $u_2 = \beta_2L_2$ are the deflections at the end points of the long and the short beam sections, respectively. \mathcal{M}_e is Young's modulus of elasticity for the wood being used for the beam and \mathcal{I} the second moment of area for the beam profile. Lengths and masses are independent parameters in the equations of motion, but (9) with a given β_2 forms a bond between M and L_2 that imply mutual scaling of masses and linear dimensions. The beam diameter D is given by

$$m_b = \rho_d \frac{\pi}{4} D^2 (L_1 + L_2), \quad (10)$$

where ρ_d is the density of the selected wood and this leads to a particular scaling for D .

The strain S at a position along the beam is half the diameter, $D/2$, times the curvature which is largest at the pivot where

$$S = \frac{D}{2} \frac{MgL_2}{\mathcal{M}_e\mathcal{I}} = \frac{3D}{2L_2} \beta_2. \quad (11)$$

The stress σ of the beam is related to the strain by $\sigma = \mathcal{M}_e S$, and the modulus of rupture is the upper limit for the stress beyond which the wood breaks. This is often near 1% of \mathcal{M}_e , so to stay on the safe side we take $S^{max} \ll 1/100$. A typical value of D/L_2 is 1/3 so $S^{max} \simeq 1/600$ for $\beta_2 = 1/300$, which is taken to be the maximum allowed bending and used throughout except when the value is specified explicitly. It is possible to use fixed S^{max} instead of fixed β_2 to control beam strength. This implies a different scaling, however, and is not pursued here.

Young's modulus and the density of strong wood are taken to be $\mathcal{M}_e = 12\text{GPa}$ and $\rho_d = 700\text{kg/m}^3$, respectively. The maximum bending, a dimensionless constant K and two useful material constants that depend on gravity are

$$\begin{aligned} \beta_2 &= 1/300 & K &= \frac{l+1}{\mu_b} \\ k_M &= \frac{4\pi}{3} \frac{g\rho_d^2}{\mathcal{M}_e} = 1.68 \cdot 10^{-3} \text{ kg/m}^4 \\ k_D &= \frac{16}{3} \frac{g\rho_d}{\mathcal{M}_e} = 3.06 \cdot 10^{-6} \text{ 1/m} . \end{aligned} \quad (12)$$

The bond between L_2 and M in (9), the expression for the beam mass in (10) and the constants in (12) lead to scaling relations for L_2 , M , T and D

$$M = K^2 \frac{k_M}{\beta_2} L_2^4, \quad T = K^2 \frac{k_M}{\beta_2} g \tau_e L_2^5 \quad \text{and} \quad D = \sqrt{K \frac{k_D}{\beta_2}} L_2^{3/2}. \quad (13)$$

The remaining parameters scale according to the relations in (5) and (7). Thus, lengths are proportional to L_2 , masses to L_2^4 , energies to L_2^5 and D to $L_2^{3/2}$.

For a selected material and allowed bending, we have now seen that given values of (l, l_4, μ_b, μ) and a single absolute parameter determine an engine completely, but a problem arises with a given capacity (R, T) , because not only one but two absolute parameters are given. This leads to inconsistent values of other absolute parameters including m . The situation may be resolved iteratively, however, if the inconsistencies are not too big: The kinetic energy and range of the projectile are related approximately by $T \simeq \frac{1}{2}mgR$, so if m is off by Δm at the given R , then $\Delta T/T \simeq \Delta m/m = \Delta\mu/\mu$, and μ can then be adjusted (iteratively if needed) to deliver the desired T . A given capacity (R, T) thus necessitates adjustment of μ and reduces the number of free parameters from four to three. Random selection of (l, l_4, μ_b) , however, is not likely to result in a particularly good design, so a criterion for optimization is needed.

5. Quality function \mathcal{Q} , force factor \mathcal{F} and optimization procedure

Two important, dimensionless variables have not yet been defined. One is the quality function \mathcal{Q} and the other a measure of the reaction forces within the engine \mathcal{F} . We first consider \mathcal{Q} . It must increase with parameters such as $\tilde{\rho} = R/L_1$, $\mu \simeq 2T/(MgR)$ and $\epsilon = T/\Delta U$, because they measure, respectively, range in terms of size L_1 , kinetic energy relative to weight M for a given range R , and efficiency, but \mathcal{Q} must also be a decreasing function of internal forces that cause wear and tear on the engine. It could therefore have the form

$$\mathcal{Q} = \frac{\tilde{\rho}\mu\epsilon}{\mathcal{F}}, \quad (14)$$

where \mathcal{F} needs to be defined. The balance between the factors in (14) can be changed by raising them to suitable powers different from one, and other factors can be included. We continue with (14) and take it as the definition of \mathcal{Q} .

The factor \mathcal{F} must represent all internal forces. This is done by selecting the sling tension \mathbf{F}_S and the force on the frame at the fulcrum \mathbf{F}_R . The tension \mathbf{F}_S is measured by the largest value of the component perpendicular to the beam $F_{S\perp}$, which is reached shortly before the release time t_r . The reaction \mathbf{F}_R is measured by its maximum value F_R . This is seen at the time t_m when the initial fall of the counterweight is slowed down the most, but we also include the horizontal component F_{Rh} of \mathbf{F}_R . This goes through two extrema in opposite directions and in rapid succession. The extrema are most often of comparable size and measured by their numeric sum $\Delta F_{Rh} = |F_{Rh}(t_1)| + |F_{Rh}(t_2)|$, where $t_1 < t_m$ and $t_2 > t_m$. With these variables, \mathcal{F} is defined by the geometric mean

$$\mathcal{F} = \left(\left(\frac{F_{S\perp}}{mg} \right)^2 \frac{F_R}{Mg} \frac{\Delta F_{Rh}}{Mg} \right)^{1/4}, \quad (15)$$

which balances sling tension and reaction forces. The quantity ΔF_{Rh} measures the forces that tend to tilt and move the engine during a shot. If this were allowed, it would be a sink of mechanical energy but is prevented by a sufficiently strong and heavy support, often in the form of a large trestle.

When the equations of motion are integrated, the inner movement of the machine is known completely. All internal forces and torques including those in (15) can then be determined by the use of Newton's second laws for translation and rotation, respectively. One always finds $F_{S\perp} \gg mg$, so the apparent weight $m_{dyn} = F_{S\perp}/g$ carried by the long beam section rises to values much larger than m . F_R is typically a few times Mg , ΔF_{Rh} always amounts to a large fraction of Mg .

The equations of motion do not include the release mechanism for the projectile. The integration in phase II can therefore be extended sufficiently in time to include the maximum of \mathcal{Q} , and any moment can subsequently be perceived as a virtual time for release. The instant t_r at which \mathcal{Q} reaches its maximum is taken as the actual release time, and the scaled parameters in (7) are evaluated here.

Finding the maximum of \mathcal{Q} for given capacity (R, T) and maximum bending β_2 implies following a procedure that may seem complicated and tedious, but it is not difficult to implement numerically. It includes the following steps

- 1) A box in (l, l_4, μ_b) -space and values μ_1 and μ_2 are carefully selected to match the desired capacity (R, T) and bending β_2 . This requires exploratory calculations.
- 2) A design (l, l_4, μ_b) is chosen at random within the box and the equations of motion solved twice. First with μ_1 returning T_1 , then μ_2 returning T_2 .
- 3) μ_1 and μ_2 are selected in step 1 such that $T_1 < T < T_2$ so linear interpolation determines an improved $\mu = \mu_3$ that returns T_3 .
- 4) This is iterated until $|T - T_i|/T < 10^{-3}$. Good selections in step 1 makes the convergence fast. \mathcal{Q} is calculated after the last iteration.
- 5) A new set (l, l_4, μ_b) is selected as in step 2 and the procedure repeated until the maximum of \mathcal{Q} is localized.

6. Optimization in vacuum

The procedure for localizing the maximum of \mathcal{Q} is illustrated in figure 2. The three figures in the lower panel show the same 10^3 calculated \mathcal{Q} -values for randomly selected design (l, l_4, μ_b) projected on the respective planes. The intervals are broad and relative drops down to 50% of a clear maximum are seen. The three figures in the upper panel

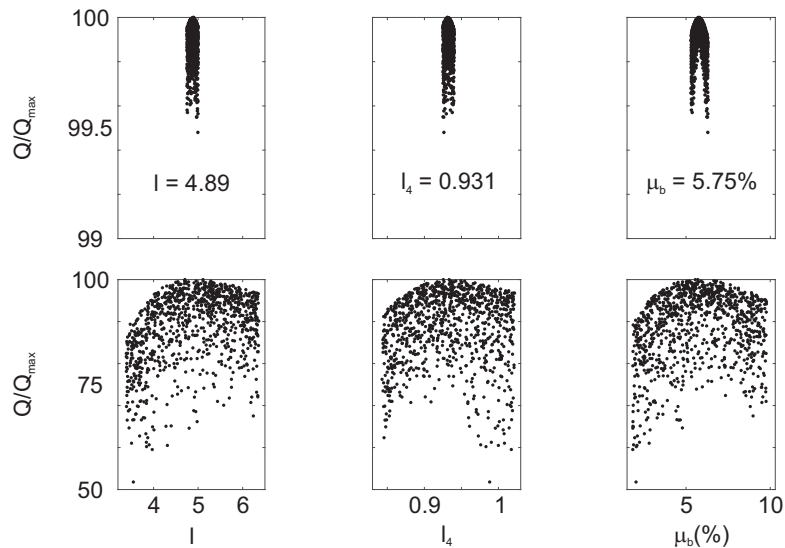


Figure 2. Q/Q_{max} in % as function of l , l_4 and μ_b . Upper panels, narrow intervals around maximum and small drops. Lower panels, wider intervals and much larger drops. $F = 1$ and capacity: $R = 240\text{m}$ and $T = 26\text{kJ}$.

also show 10^3 values of \mathcal{Q} , but for parameters selected from much narrower intervals to localize the maximum more precisely. The intervals show that \mathcal{Q} depends much more strongly on l_4 than on l or μ_b , and a fit of the \mathcal{Q} -values in the upper panel by a quadratic form shows that the principal axis in the direction of maximum curvature lies very close to the direction of l_4 .

A total of $\simeq 10^4$ integrations were required to accumulate the 2×10^3 points in the figure: For each randomly selected design (l, l_4, μ_b) it took on the average 5 integrations to adjust μ for the desired capacity (R, T) . These are the iterations mentioned in step 4 of the procedure in section 5. Many more than 10^4 integrations were actually done because exploratory integrations are also required as mentioned in step 1.

Figure 2 serves as an illustrative example, but a slightly different and more efficient practice was followed in most calculations. The interpolations in step 3 require fewer steps when T is replaced by $\log(T)$, and relatively wide parameter intervals at the outset were narrowed systematically around a running estimation of the maximum position such that optimal parameter values could be found with sufficiently accurately already after a thousand integrations or so.

6.1. Analytical expressions for absolute parameters

According to the results on scaling in section 3, the optimal design at (R_0, T_0) is also the best along the curve $T/T_0 = (R/R_0)^5$ in the (R, T) -plane. This is a straight line in a logarithmic representation and a rotation expressed in matrix form by

$$\begin{Bmatrix} X \\ Y \end{Bmatrix} = \frac{1}{\sqrt{26}} \begin{Bmatrix} 5 & -1 \\ 1 & 5 \end{Bmatrix} \begin{Bmatrix} \log(R/R_0) \\ \log(T/T_0) \end{Bmatrix} \quad (16)$$

defines coordinates (X, Y) for which the scaling applies at constant X as illustrated in figure 3. A finite number of optimizations along the X -axis followed by interpolation

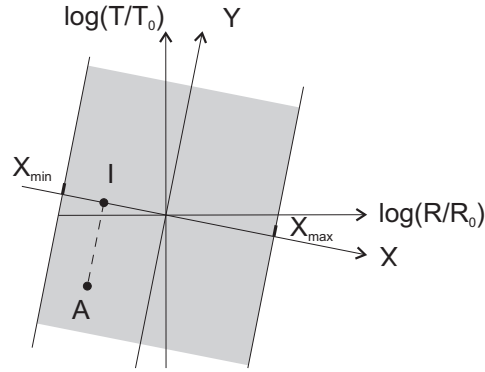


Figure 3. Coordinates (X, Y) . Scaling along lines of constant X .

and scaling determine optimal engines over a continuous region limited only by the range of X -values covered (the gray area in figure 3). Suppose, as an example, that one wishes to find the best engine at the point A with coordinates (R, T) . Scaling connects A to the point I with (X, Y) coordinates

$$X_i = \frac{1}{\sqrt{26}} \left(5 \log \frac{R}{R_0} - \log \frac{T}{T_0} \right) \quad \text{and} \quad Y_i = 0. \quad (17)$$

This point will most likely not belong to the set of calculated points, but linear interpolation with the two neighboring points on the X -axis gives a good estimate. Interpolation is tedious and requires tables for each parameter. It can be avoided, however, by the introduction of a set of analytical functions $f_Z(X)$, where index Z refers to any one of the absolute parameters for the trebuchet. We take M as an example and find because masses are proportional to lengths for constant X (13)

$$\frac{M}{M_0} = f_M(X) \left(\frac{R}{R_0} \right)^4, \quad (18)$$

where $f_M(X)$ is found from the integrations along the X -axis. For any (R, T) , the interpolation point X_i on the X -axis is given by (17), so M is a function of (R, T) alone. It turns out that $f_M(X)$ can be represented closely over broad ranges of X by the form

$$f_M = a_M \exp(b_M \sqrt{26} X) \quad (19)$$

where a_M and b_M are adjustable constants. After insertion of (19) in (18) and use of (17) one finds

$$\frac{M}{M_0} = a_M \left(\frac{R}{R_0}\right)^{4+5b_M} \left(\frac{T}{T_0}\right)^{-b_M} \quad \text{with} \quad a_M \simeq 1. \quad (20)$$

Expressions similar to (18), (19) and (20) apply for all other absolute parameters Z , so

$$\frac{Z}{Z_0} = f_Z(X) \left(\frac{R}{R_0}\right)^{n_Z} \quad \text{where} \quad \begin{cases} n_Z = 1 & \text{for } L_1, L_2 \text{ and } L_4 \\ n_Z = 3/2 & \text{for } D \\ n_Z = 4 & \text{for } M, m \text{ and } m_b \end{cases} \quad (21)$$

or more explicitly

$$\frac{Z}{Z_0} = a_Z \left(\frac{R}{R_0}\right)^{p_Z} \left(\frac{T}{T_0}\right)^{q_Z} \quad \text{where} \quad \begin{cases} p_Z = n_Z + 5b_Z \\ q_Z = -b_Z \end{cases} \quad (22)$$

The result of fitting the form (21) to the seven parameters are shown in figure 4. The

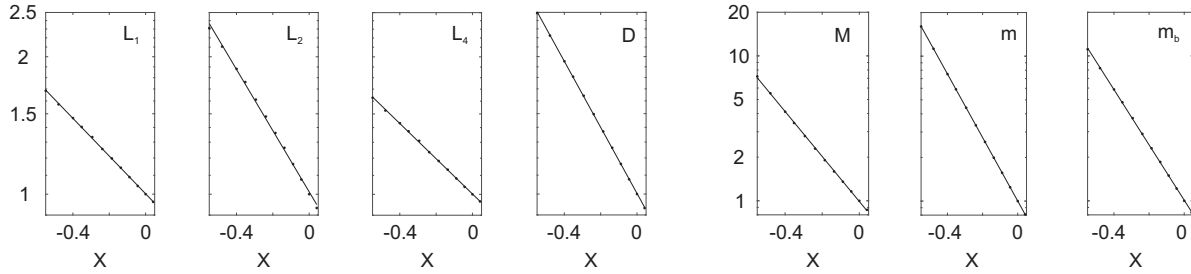


Figure 4. Full points, calculated values of $(Z/Z_0)/(R/R_0)^{n_Z}$ vs X . Straight lines, fits by $f_Z(X)$. Semi-logarithmic plots. $R_0 = 240\text{m}$. $T_0 = 26\text{kJ}$. $\theta_i = 30^\circ$. $F = 1$.

functions f_Z are straight lines in the chosen semi-logarithmic representation. They are seen to represent the calculated values accurately so the analytical expression (22) gives a very good estimate of the optimal value for the chosen parameter for any desired capacity (R, T) with X -value within the interval covered. All data for lengths are plotted at the same scale and so are the data for masses. This facilitates comparison within each group, but note that the length scale covers a factor $\simeq 2.5$ variation whereas the mass scale covers a factor $\simeq 20$ variation.

Equation (22) is linear in a logarithmic representation. The relation between (R, T) and two absolute parameters Z_i and Z_j from (4) can therefore be expressed by

$$\begin{Bmatrix} \log(Z_i/Z_{i0}) \\ \log(Z_j/Z_{j0}) \end{Bmatrix} = \begin{Bmatrix} p_{Z_i} & q_{Z_i} \\ p_{Z_j} & q_{Z_j} \end{Bmatrix} \begin{Bmatrix} \log(R/R_0) \\ \log(T/T_0) \end{Bmatrix}, \quad (23)$$

where we have use $\log(a_Z) \simeq 0$. The equation can be inverted provided the determinant $\mathcal{D}_{ij} = p_{Z_i}q_{Z_j} - q_{Z_i}p_{Z_j}$ is different from zero, and if so

$$\begin{Bmatrix} \log(R/R_0) \\ \log(T/T_0) \end{Bmatrix} = \frac{1}{\mathcal{D}_{ij}} \begin{Bmatrix} q_{Z_j} & -q_{Z_i} \\ -p_{Z_j} & p_{Z_i} \end{Bmatrix} \begin{Bmatrix} \log(Z_i/Z_{i0}) \\ \log(Z_j/Z_{j0}) \end{Bmatrix}. \quad (24)$$

Absolute parameters (Z_i, Z_j) and (Z_k, Z_l) are related two-by-two if (R, T) is eliminated from (23) and (24), and (X, Y) can be included by the use of (16).

Table 1 shows constants derived from the fits in figure 4. The interval of X -values for which the constants apply is also given. Constants from other fits of similar quality to data with $X > 0$, $F = 2/3$ and $\theta_i = 40^\circ$ are also included. The data with $X > 0$ and $F = 1$ show a narrow region of X from 0.3 to 0.4 with competing optimized design.

X	θ_i	F		L_1	L_2	L_4	D	M	m	m_b
			Z_0	3.90m	0.80m	3.62m	0.22m	2158kg	20.6kg	124kg
	30°	1	a_Z	1.00	1.02	1.00	1.00	0.98	1.00	1.01
-0.55	30°	1	p_Z	0.0654	-0.5013	0.1243	-0.1299	0.4830	-0.9481	-0.3045
0	30°	1	q_Z	0.1869	0.3003	0.1752	0.3260	0.7034	0.9896	0.8609
lb	30°	1	a_Z	0.9967	1.0104	0.9937	1.0025	0.9893	0.9988	1.0023
0	30°	1	p_Z	0.0816	-0.7853	0.1979	-0.2069	0.7431	-0.9613	-0.4591
0.40	30°	1	q_Z	0.1837	0.3571	0.1604	0.3414	0.6514	0.9923	0.8918
ub	30°	1	a_Z	1.12	1.21	1.31	1.05	0.841	1.01	1.25
0.30	30°	1	p_Z	-0.1385	-1.0423	-0.1625	-0.2839	0.9490	-0.9757	-0.8238
0.57	30°	1	q_Z	0.2277	0.4084	0.2325	0.35678	0.6102	0.9951	0.9647
	30°	2/3	Z_0	3.97m	0.67m	3.58m	0.21m	2590kg	20.7kg	112kg
	30°	2/3	a_Z	1.00	1.01	1.00	1.00	0.99	1.00	1.00
-0.55	30°	2/3	p_Z	0.08611	-0.3131	0.1640	-0.0856	0.2839	-0.9459	-0.1487
0	30°	2/3	q_Z	0.1828	0.2626	0.1672	0.3171	0.7432	0.9892	0.8297
	30°	2/3	a_Z	1.00	1.00	1.00	1.00	1.00	1.00	1.00
0	30°	2/3	p_Z	0.0400	-0.6865	0.1465	-0.1851	0.6328	-0.9672	-0.4210
0.57	30°	2/3	q_Z	0.1920	0.3373	0.1707	0.3371	0.6735	0.9934	0.8842
	40°	2/3	Z_0	4.13m	0.63m	3.47m	0.21m	2925kg	20.7kg	116kg
	40°	2/3	a_Z	1.00	1.00	1.00	1.00	1.00	1.00	1.00
-0.52	40°	2/3	p_Z	0.0857	-0.3429	0.2012	-0.0944	0.3080	-0.9481	-0.1641
0	40°	2/3	q_Z	0.1829	0.2686	0.1598	0.3189	0.7384	0.9896	0.8328
	40°	2/3	a_Z	1.00	1.01	1.00	1.00	0.99	1.00	1.01
0	40°	2/3	p_Z	0.0672	-0.6765	0.2546	-0.1858	0.6100	-0.9666	-0.3880
0.52	40°	2/3	q_Z	0.1866	0.3353	0.1491	0.3372	0.6780	0.9933	0.8776

Table 1. Constants in Equation (22) with $R_0 = 240\text{m}$ and $T_0 = 26\text{kJ}$. Limits on X . Overlap for $0.3 < X < 0.4$. lb: lower branch. ub: upper branch.

6.2. Two branches of optimized design

Two different optimized design compete at X between 0.3 and 0.4 when $\theta_i = 30^\circ$ and $F = 1$ as seen in table 1. In this narrow range of X , the quality function $\mathcal{Q} = \mathcal{Q}_X(l, l_4, \mu_b)$ shows two maxima, which are seen most easily when the calculations are projected on the (l_4, \mathcal{Q}) -plane (as in middle figure in lower panel of figure 2). The maximum belonging to the lower branch with $X_{max} = 0.40$ dissolves near X_{max} . The other maximum on the upper branch with $X_{min} = 0.30$ emerges near X_{min} , and the two maxima are equally high at $X = X_d$, where $X_d \simeq 0.34$. \mathcal{Q} is continuous at X_d , but all other parameters are discontinuous at this point with steps that depend on X but not

on Y . The size of the step S_Z follows from (16) after inversion and (23). It reads

$$S_Z = \frac{Z_{ub}}{Z_{lb}} = \frac{a_{Z_{ub}}}{a_{Z_{lb}}} \exp\left(\frac{5pZ_{ub} - qZ_{ub} - 5pZ_{lb} + qZ_{lb}}{\sqrt{26}} X_d\right), \quad (25)$$

where the constants are taken at the two branches. The largest step is $S_{L_4} = +16.3\%$. Others are $S_{L_1} = +4.4\%$ and $S_M = -8.7\%$ while m increases by less than 1%.

For X near X_d we find after expansion of the exponential function

$$l_4 = \frac{L_4}{L_1} = \begin{cases} 0.965(1 + 0.119(X - X_d)) & \text{on lower branch} \\ 1.075(1 - 0.024(X - X_d)) & \text{on upper branch,} \end{cases}$$

so the relative sling length is less than one and increasing on the lower branch, and larger than one and decreasing at a smaller rate on the upper.

The configuration of an optimized trebuchet at the best time for release of the projectile is also qualitatively different on the two branches. On the lower branch, the beam has not yet crossed the vertical direction, but on the upper branch, it has just crossed it for the first time. Competing designs are found in a very narrow interval of X near 0.58 when $\theta_i = 30^\circ$ and $F = 2/3$, and for other θ_i and F as well.

6.3. Frequency of optimized design

Equation (23) can be expanded to cover the six absolute parameters Z_i listed in (4)

$$\left\{ \log(Z_i/Z_{i0}) \right\}_{6 \times 1} = \left\{ pZ_i \quad qZ_i \right\}_{6 \times 2} \begin{Bmatrix} \log(R/R_0) \\ \log(T/T_0) \end{Bmatrix}_{2 \times 1}, \quad (26)$$

where the dimensions of the matrices are given explicitly. Thus, optimized absolute parameters are limited to a two dimensional hyperplane imbedded in a space of six dimensions. This is the vector space spanned by the two column vectors in the 6×2 matrix. Good designs are found near every optimized design, so by including these the plane expands in all directions to form an object of final but very small volume in the huge six dimensional space. This illustrates the rarity of good designs and how difficult it is to find them.

We further illustrate the difficulty by examining a standard set of four parameters chosen by Denny to represent a large trebuchet [8]. The standard parameters are

$$L_b = 12\text{m}, \quad M = 10\,000\text{kg}, \quad m = 100\text{kg} \quad \text{and} \quad m_b = 2000\text{kg},$$

where $L_b = L_1 + L_2$ is the beam length. They can be paired two-by-two in six ways and the capacity (R, T) was calculated for each by the use of (24) and table 1 with $\theta_i = 30^\circ$ and $F = 2/3$. Only one of the six pairs results in a meaningful capacity and a value of X within the limits in table 1. This is $M = 10\,000\text{kg}$ and $m = 100\text{kg}$ with $R = 288\text{m}$ and $T = 152\text{kJ}$ that implies $X = -0.17$. The optimized beam length for this capacity calculated by the use of (22) is $\simeq 6.6\text{m}$ which is quite small when compared to the standard of 12m, and the weight of the beam $\simeq 475\text{kg}$ is even smaller in relative terms compared to 2000kg. The efficiency of the optimized engine is $\simeq 92\%$.

A trebuchet with the standard parameters does not maximize \mathcal{Q} , but it works and Denny [8] finds a maximum range in air of 360m and a projectile velocity at release

of 63m/s. This result is listed in the first row of table 2 and data from present *ab initio*

	θ_i	β_2 %	F	\mathcal{Q} %	ϵ %	L_b m	H m	L_4 m	M ton	m kg	m_b kg	R m	T kJ
Denny	45^0					12	6.15	7.9	10	100	2000	360	
Present	45^0	0.66	0.93	1.7	48.4	12	6.15	7.9	10	100	2000	425	224
Max \mathcal{Q}	45^0	0.66	0.93	7.0	91.4	8.67	5.25	6.19	13.3	101	629	425	224
Max \mathcal{Q}	30^0	0.33	1	7.8	93.3	7.15	5.23	5.69	13.3	101	647	425	224
Max \mathcal{Q}	30^0	0.33	2/3	6.7	92.2	7.06	5.30	5.57	15.7	101	591	425	224
Model	30^0	0.33	2/3	6.7	92.2	1.33	1.00	1.05	19.9kg	0.127	0.745	80.0	53.1

Table 2. Comparison of design. Denny: R from [8] for standard parameters. Present: Present results with Denny’s parameters. Max \mathcal{Q} : Design at maximum \mathcal{Q} by *ab initio* calculations and given (R, T) . Model: Scaled values, Equation (13).

calculations are given in the second row. The values of β_2 and F follow from Denny’s data. The range in vacuum of 425m results from a release velocity (64m/s) in full agreement with Denny’s. The different ranges are explained by aerodynamic losses and different definitions of range. Air drag reduces the vacuum range to 380m by the same assumptions as used by Denny who also measures range by the distance from the release point to the point where the projectile dips below the release height. The release is at a height of 20.2m and at a position 6.0m behind the pivot. The range by Denny should therefore be compared with $380\text{m} - 20\text{m} + 6\text{m} = 366\text{m}$, which again shows good agreement. The vacuum value of kinetic energy at target is 224kJ and the efficiency 48.4%.

The remaining results in table 2 show design that maximize \mathcal{Q} at the capacity 425m and 224kJ that follows from the standard parameters. The first of these are for Denny’s values of θ_i , β_2 and F , and it shows a shorter and lighter beam (L_b, m_b), a smaller height of the pivot H and a heavier counterweight M . The efficiency ϵ of the engine is increased by more than a factor of two, so loading requires less than half the energy needed for loading the standard machine. The present standard values of θ_i , β_2 and F , and the more realistic $F = 2/3$ are used in the next two rows. The steeper initial beam position and selection of a stronger beam results in further shortening of the beam, almost unchanged pivot height, still heavier counterweights and slightly increased efficiencies. The efficiencies of the optimized engines in table 2 are all somewhat larger than 90%. This is in clear contrast to an apparent consensus in the literature on an upper limit near 70% [7, 8].

The last row in table 2 shows dimensions of a small trebuchet found by scaling the one just above. The small engine can be handled safely by only a couple of people, but the small mass of the projectile increases the aerodynamic sensitivity. Approximately equal relative losses can be obtained, however, by selecting a projectile material of higher density than stone. A simple estimate gives $\rho/\rho_{stone} \simeq 2.3$, so iron would do.

7. Trebuchets of archaeological interest

The cases selected to illustrate the present results were chosen by their archaeological significance. The first relate to the sieges of Alcalá la Vieja in 1118 by Christian forces and of Saone in 1188 by Saladin's army. Others are inspired by drawings in the sketchbook of Villard de Honnecourt [10] from the early 13th century.

The optimizations most often take outset in desired ranges R and known or assumed projectile masses m . Optimized parameters can then be found by the use of (22) to first determine T , whereafter the remaining parameters follow from (23). Another starting point is an assumed beam length and partitioning, which determines L_1 and L_2 . The capacity then follows from (24) and the remaining optimized parameters from (23).

The results show strong variation of mass with size, *i.e.* $M \propto L_2^4$ by (13). This is not immediately understandable, so the optimized design to follow are most likely smaller and heavier than expected. Simple proportionality, *i.e.* $M \propto L_2$, is more straightforward, but is not consistent with the present analysis. See chapter 2 of [4] for a recent discussion of scaling based on intuition and *ad hoc* estimates.

7.1. Alcalá la Vieja and Saone

The ranges listed in the first three rows of table 3 are central to the discussion by Galán and Galán [6] of the siege of Alcalá la Vieja, where strategically advantageous locations for trebuchets were examined outside the range of arrows fired from the fortress (*i.e.* $\simeq 140\text{m}$). Stones found in the area and most likely used as projectiles

Site	Level m	R m	T kJ	L_1 m	L_2 m	L_4 m	D m	M tons	m_b kg	ϵ %	v m/s	h m	A
Ca	(-15)	150	40.3	4.13	0.88	3.55	0.25	3.11	174	90.0	37.7	10.0	40.3 ⁰
Ma	(-54)	480	124	5.50	0.71	5.15	0.31	11.5	334	92.8	68.5	13.8	39.1 ⁰
Ma	-54	426	111	5.36	0.75	4.96	0.31	9.70	320	92.5	64.5	13.5	39.1 ⁰
Sa	(-20)	250	66.0	4.72	0.85	4.19	0.28	5.16	242	91.4	49.1	11.7	39.7 ⁰

Table 3. Optimized trebuchets with $\theta_i = 30^\circ$, $F = 2/3$ and $m = 50\text{kg}$ stones. First three rows: Siege of Alcalá la Vieja with Catalanes site (Ca), and Malvecino site (Ma). Fourth row: Siege of Saone. Level: Level of target relative to trebuchet.

typically weigh around 50kg. The energies T that follow from R and m give values of X within the limits in table 1. Algebraically determined optimized parameters then found are given in the central columns of table 3. The parameters to the right are efficiencies ϵ and initial conditions for the projectile's ballistic trajectory towards the target, which are speed v , height h and climb A at release. The engines are elevated relative to the targets, but this is ignored in most cases (and clarified by placing the target level in parenthesis). The lower level of the targets then more than compensates for aerodynamic losses of range and energy along the projectile path. In the example without parenthesis, the aim is shortened by the difference of level, and optimized parameters are then found as before by assuming no difference of level. The projectile flies past the shortened aim

of 426m and reaches the lower level of the target at 481m. The approximate procedure thus overshoots the range by just one meter. The kinetic energy increases from 111kJ at zero level to 137kJ at target due to gravity. The potential energy stored in the engine before the shot is $111\text{kJ}/0.925=120\text{kJ}$, *i.e.* less than the energy at target.

The trebuchets erected at the Catalanes site were hybrids of traction and fixed counterweight engines with beam lengths near 9.5m [6]. The optimized realization in table 3 is much smaller. Having had a small engine like this at their disposal would have been a great advantage for the leaders of the campaign because it makes transportation and erection much easier. The heavy counterweight of $\simeq 3$ metric tons can be a light box that is taken apart for transportation, then reassembled and loaded with rocks and soil at a new deployment.

The Melvecino site was ruled out [6] because of the long distance to the fortress, but a trebuchet of manageable size placed at Malvecino could indeed have bombarded the fortress with 50kg stones. However, the required counterweight of 11.5 tons (or 9.7 tons) is challenging. The siege of Alcalá la Vieja took place early in the 12th century when counterweight trebuchets were still under development and perhaps had not yet matured into a stage where such heavy counterweights could be used.

The data in the fourth row of table 3 relate to the siege of Saone. A likely position for trebuchets exists at a distance of 250m from the fortifications of the castle [5], and an optimized engine that covers this range is seen to deliver 66kJ to the target. In a discussion of the siege by Fulton *et al.* [5] it is concluded that the trebuchets deployed there could not have been breaching weapons at this early stage of development, but we have seen that well constructed engines of limited size and weight could indeed have bombarded the fortifications by 50kg stones arriving at $\simeq 185\text{km/h}$.

The siege of Saone took place only 70 years after the siege of Alcalá la Vieja, but they are not easily compared. The fall of Alcalá la Vieja, located close to Madrid in Spain, was part of the reconquest of Spain whereas Saone, located in Syria close to the Mediterranean Sea, was taken during Saladin's Syrian campaign.

7.2. Sketchbook of Villard de Honnecourt

The sketchbook of Villard de Honnecourt, which dates back to the early 13th century, has a drawing of the sole (or base framing) of a trebuchet and a description of a chest full of earth which is the counterweight. Both have detailed length indications. The sizes of sole and chest suggest beam lengths and counterweights of up to 10m and thirty metric tons, respectively.

Chevedden suggests that a huge trebuchet like this can throw a 100kg stone more than 400m [3]. Following this suggestion, we take $m = 100\text{kg}$ and $R = 450\text{m}$. The energies T that follow allow the optimized parameters in the first rows of table 4 to be found algebraically. $F = 1$ in the first row is the ideal case and $F = 2/3$ in the next two the more practical. The initial beam angle $\theta_i = 40^\circ$ is perhaps also more appropriate than $\theta_i = 30^\circ$. The beam lengths close to 7m seem short when compared to the sole,

n	F	θ_i	R m	T kJ	L_1 m	L_4 m	M tons	m kg	m_b kg	L_b m	l	ϵ %	\mathcal{Q}_n %
1	1	30^0	450	235	6.13	5.80	14.3	100	660	7.21	5.68	93.1	7.41
1	2/3	30^0	450	234	6.20	5.69	16.9	100	601	7.12	6.77	92.6	6.43
1	2/3	40^0	450	234	6.48	5.55	19.1	100	622	7.35	7.51	91.6	5.55
5	1	30^0	450	235	6.31	6.68	15.6	101	611	7.26	6.64	97.5	6.38
0	1	30^0	450	235	6.60	6.04	13.4	98.3	807	7.85	5.29	87.8	8.11

Table 4. Design relating to Villard de Honnecourt. Quality function \mathcal{Q}_n in (27).

and counterweights of less than 20 tons are also relatively small in comparison with the maximum of 30 tons. The variations of linear size in going from $F = 1$ to $2/3$ and from $\theta_i = 30^0$ to 40^0 are modest, but M increases more significantly. Finally, the counterweight was propped in row 2. This has only a small effect on ϵ with a maximum of 93.0% at $\psi_i = -4.6^0$ because the initial counterweight motion is slightly better.

The two lowest rows in table 4 show optimized design obtained by the use of the modified quality function

$$\mathcal{Q}_n = \frac{\tilde{\rho}\mu\epsilon^n}{\mathcal{F}} \quad \text{with} \quad n \geq 0, \quad (27)$$

which is the same as (14) when $n = 1$. There is more emphasis on efficiency ϵ when $n > 1$ and less when $n < 1$. We see that ϵ increases from 93.2% at $n = 1$ to 97.5% at $n = 5$ and decreases to 87.8% at $n = 0$ with only small adjustments of the engine. The most remarkable is the change of relative sling length l_4 to a value larger than one at $n = 5$. This reveals a transition to a qualitatively different engine (see discussions in section 6.1 and Appendix B).

Many trebuchets built early on could throw heavy stones a good distance, but their precise dimensions are unknown. A trebuchet with proportions derived from the dimensions of the sole in the sketchbook is shown in a semi-realistic drawing included as figure 26 in a commented facsimile version of the sketchbook published in 1859 [10]. As measured on the drawing, the beam is divided by the pivot into two lengths with ratio $l = L_1/L_2 \simeq 4.5$, and the initial beam angle is $\theta_i \simeq 25^0$, but figure 27 in [10], which serves to illustrate an explanation of the action of a trebuchet, shows a different initial configuration with $\theta_i \simeq 40^0$. Table 5 shows optimized design that comply with these findings. The three cases with $\theta_i = 25^0$ or 40^0 and $F = 1/2$ were calculated *a priori*. The results illustrate the variation in going from the ideal F -value of 1 to the more realistic $2/3$ or $1/2$, and also the consequences when θ_i is varied from 30^0 to 25^0 or 40^0 . The variations are not very dramatic and the efficiencies are larger than 90% in all cases except when $F = 1/2$ and ϵ dips just below 90%.

The large masses of the counterweights in table 5 can be reduced to the estimated maximum of 30 tons by relatively small reductions of the linear dimensions. According to (13) one finds for small changes $\Delta R/R = \Delta L_i/L_i \simeq 1/4 \cdot \Delta M/M$ or about 8% in the worst case, where R is reduced by 22m to 275m, but T drops strongly to 102kJ. The reduction can also be implemented by variation of the allowed maximum bending β_2 of

#	F	θ_i	R m	T kJ	L_1 m	L_4 m	M tons	m kg	m_b kg	L_b m	l	ϵ %	\mathcal{Q} %
1	1	25^0	426	677	7.36	7.00	26.8	301	1696	9	4.5	93.3	10.4
2	1	30^0	407	641	7.36	6.80	26.0	298	1682	9	4.5	92.9	10.2
3	1	40^0	341	540	7.36	6.20	23.7	299	1589	9	4.5	91.5	10.2
4	1	30^0	540	700	7.62	7.16	33.4	248	1605	9	5.5	93.2	7.71
5	2/3	30^0	401	726	7.62	6.76	34.9	343	1653	9	5.5	91.6	8.79
6	2/3	30^0	482	752	7.74	6.98	38.7	299	1623	9	6.0	92.0	7.55
7	1/2	30^0	297	858	7.69	6.41	45.9	538	1746	9	6.0	88.1	9.01

Table 5. Design relating to Villard de Honnecourt. Given L_b and l .

the beam. Bending is treated as a perturbation so it is not found in the equations for the inner movement in Appendix A, but only in the scaling relations (13) for lengths, masses and energies. Therefore, in case β_2 is varied while one linear dimension is kept constant (like L_b in table 5), all other linear dimensions are invariants, while all masses, the energy T and the beam cross section $(\pi/4)D^2$ are inversely proportional to β_2 . The counterweights M in table 1 are therefore reduced if β_2 is increased (or beam strength weakened for same quality of wood). Only modest reductions are necessary to bring most masses below 30 tons, but 35% is required for the heaviest and this is accomplished when β_2 is increased from 1/300 to 1/200. This leaves the range invariant at 297m while T is reduced to 572kJ, less dramatically than above. It may seem odd that a smaller M implies a larger bending. However, bending depends only on bending force Mg and beam strength $\mathcal{I} \propto D^4$ under the given conditions, and D^2 is proportional to m_b and M . The bending, which is proportional to Mg/\mathcal{I} , therefore varies like $1/M$. Similar considerations apply to variation of the material constants ρ_d and \mathcal{M}_e , or even gravity g for a trebuchet on a special mission to the moon.

8. Summery and results

The parameter space for the type of trebuchet discussed here is very large, but reduced significantly by reasonable selections of initial conditions and length of the arm for the counterweight. The six free parameters that remain are listed in (4), but further reduction is possible because the equations for the internal movement can be scaled. This leaves the four dimensionless parameters (l, l_4, μ, μ_b) in (6). A quality function \mathcal{Q} that depends only on these is defined in (14). It does not have a maximum under variation of all four parameters, but a desired capacity and limited bending of the beam imposes a constraint among the parameters that secures a maximum. This was found for many capacities and selected initial beam angles and counterweight arms. The result can be summarized by a set of constants and a simple analytical expression given in (22). The comprehensive lists in table 1 allow the determination of absolute dimensions and masses of optimized engines over a broad range of capacities. Equation (22) can also be used to link parameters two-by-two as done in several instances. This is facilitated by the methods of linear algebra. Evaluation can in every case be done simply by hand or

more effectively with a spreadsheet. This is the key result of the present study.

Two competing branches of optimized design exist in special cases. Even so, it is difficult to determine optimized design without guidelines. We explain why and illustrate this by considering a proposed standard set of parameters to represent a large trebuchet. It works but is far from optimal according to the present criteria.

A number of optimized design of archaeological interest are derived, and a clear trend is seen when the optimized dimensions are compared with the ones attributed to historical trebuchets: The optimized engines are smaller and the counterweights heavier. Internal forces are also reduced and efficiencies increased.

Appendix A. Scaled equations of internal movement

Scaled time is $\tau = (g/L_2)^{1/2}t$ and dot-notation is used for differentiation with respect to τ . Scaled lengths (l , l_4 and L) and masses (μ and μ_b) are given in (5).

Appendix A.1. Phase I. Projectile in trough.

The coupled differential equations for the motion of beam and counterweight are

$$\begin{aligned} & \left(\mu l^2 f(\theta)^2 + \frac{\mu_b}{3} (l^2 - l + 1) + 1 \right) \ddot{\theta} - L \cos(\theta - \psi) \ddot{\psi} \\ & + \mu l^2 f(\theta) \frac{df}{d\theta} \dot{\theta}^2 - L \sin(\theta - \psi) \dot{\psi}^2 \\ & + \left(\frac{\mu_b}{2} (l - 1) - 1 \right) \sin \theta = 0 \end{aligned} \quad \text{and} \quad (\text{A.1})$$

$$L \ddot{\psi} - \cos(\theta - \psi) \ddot{\theta} + \sin(\theta - \psi) \dot{\theta}^2 + \sin \psi = 0 . \quad (\text{A.2})$$

The sling angle ϕ satisfies the geometric relation

$$\cos \theta + l_4 \sin \phi = \cos \theta_i , \quad (\text{A.3})$$

where θ_i is the initial beam angle, and the functions f and $df/d\theta$ in A.1 are

$$f(\theta) = \frac{\cos(\theta - \phi)}{\cos \phi} \quad \text{and} \quad \frac{df}{d\theta} = -\frac{\sin(\theta - \phi)}{\cos \phi} + \frac{\sin^2 \theta}{l_4 \cos^3 \phi} .$$

Appendix A.2. Phase II. Projectile lifted from trough.

The three equations for the motion of beam, counterweight and sling are equation (A.2),

$$\begin{aligned} & \left(\mu l^2 + \frac{\mu_b}{3} (l^2 - l + 1) + 1 \right) \ddot{\theta} - L \cos(\theta - \psi) \ddot{\psi} - \mu l^2 l_4 \sin(\theta - \phi) \ddot{\phi} \\ & - L \sin(\theta - \psi) \dot{\psi}^2 + \mu l^2 l_4 \cos(\theta - \phi) \dot{\phi}^2 \\ & + \left(\mu l + \frac{\mu_b}{2} (l - 1) - 1 \right) \sin \theta = 0 \end{aligned} \quad \text{and} \quad (\text{A.4})$$

$$l l_4 \ddot{\phi} - l \sin(\theta - \phi) \ddot{\theta} - l \cos(\theta - \phi) \dot{\theta}^2 - \cos \phi = 0 . \quad (\text{A.5})$$

Appendix A.3. Phase III. Projectile released.

The equations for the motion of beam and counterweight are (A.4) with $\mu = 0$ and (A.2).

Appendix B. Maximizing efficiency ϵ

The function \mathcal{Q}_ϵ defined by

$$\mathcal{Q}_\epsilon = \frac{\tilde{\rho}^0 \mu^0 \epsilon}{\mathcal{F}^0} = \epsilon ,$$

has the form of a quality function, but does not qualify as such, because it does not have a maximum under variation of (l, l_4, μ_b) at a given capacity (R, T) and allowed bending β_2 . However, attempts at optimization reveals two maxima of $\mathcal{Q}_\epsilon = \epsilon$ under variation of (l_4, μ_b) with constant l . For high values of l , one maximum is found at $l_4 < 1$, the other at $l_4 > 1$ and both are increasing functions of l that appear to converge towards 1.

Table 4 with parameters relating to Villard de Honnecourt shows optimized engines with the capacity $R = 450\text{m}$ and $T = 232\text{kJ}$. Depending on the quality function used for the optimization, the efficiency ranges up to $\epsilon = 97.5\%$ for practical design parameters. Calculations with the same capacity and $\mathcal{Q} = \mathcal{Q}_\epsilon$ show an increase of ϵ above 99.5% at $l = 16.2$ on the smaller- l_4 branch and at $l = 58.5$ on the larger- l_4 branch. These high values of l and the given capacity result in absolute parameters that can not be used in practical engines (see table B1), but the dynamics is interesting from a formal point of view.

l	ϵ %	L_1 m	L_2 m	L_4 m	M ton	m kg	m_b kg	θ -180^0	ψ -1.98^0	ϕ -180^0	A 44.9^0
17	99.53	0.800	0.047	0.673	270	104	14.7	-1.95^0	-1.98^0	45.1^0	44.9^0
59	99.50	14.9	0.25	18.2	71.5	93.5	729	-1.22^0	-0.91^0	47.6^0	42.6^0

Table B1. Design with high efficiencies ϵ . $F = 1$, $\theta_i = 30^0$, $R = 450\text{m}$ and $T = 232\text{kJ}$. Angles of beam θ , counterweight ψ and sling ϕ at release. A : initial climb of projectile. First row: Smaller- l_4 branch. Second row: Larger- l_4 branch.

As l is increased, both branches show decreasing relative projectile and beam masses which ensures an initial almost free fall of the counterweight. However, the fall must stop eventually and because of the one-sided focus on high efficiency, the relative parameters (l_4, μ_b) are adjusted such that the descending motion is transformed smoothly at the last moment into an oscillatory motion of small amplitude.

This is seen most clearly in the limit $l \rightarrow \infty$ on the smaller- l_4 branch where one of the two equations for the phase III motion takes the form

$$\ddot{\theta} - L \cos(\theta - \psi) \ddot{\psi} - L \sin(\theta - \psi) \dot{\psi}^2 - \sin \theta = 0 ,$$

while the other is unchanged. The two equations are solved by

$$(L + 1) \ddot{\psi} + \sin \psi = 0 \quad \text{and} \quad \theta - \psi = \pi ,$$

which for small amplitudes are harmonic oscillations. These have dimensionless frequency $\{1/(L + 1)\}^{1/2}$ or in absolute terms $\{g/(L_2 + L_3)\}^{1/2}$. The counterweight and beam thus swing in phase relative to the pivot as a quasi-solid body with pendulum length $L_2 + L_3$. The transition from free fall of the counterweight to harmonic motion

takes place over a very short period of time. Counterweight and beam slow down during this period without ever stopping and go into the common oscillating mode such that the combined motion is towards the equilibrium point. The reaction force from the fulcrum rises to a very high level during this transition.

A closer inspection of the motion for large but finite l reveals an internal oscillation of high frequency on top of the harmonic component. The angle $\theta - \psi$ oscillates around π with very small amplitude as though the quasi-solid rings. This is understood by including small terms as perturbations. When the beam motion is not totally forced by the heavy counterweight it depends on the beam's moment of inertia relative to the pivot, but the torque on the beam is still dominated by the heavy counterweight of scaled mass 1. The scaled moment of inertia is $\mathcal{I}_P = 1/3 \cdot \mu_b (l^2 - l + 1)$ so the frequency of small oscillations is $\omega \simeq \mathcal{I}_P^{-1/2}$ and a closer analysis gives the more precise expression $\omega = \{L/(L + 1) \cdot \mathcal{I}_P\}^{-1/2}$.

For $l = 17$ in table B1, the reaction force at the culcrum reaches nearly $10Mg$, the tension of the sling rises to $350mg$ shortly before release, and the internal oscillations have $f = 42.2\text{Hz}$. Further, as seen in table B1 the configuration at release is almost vertical, and the projectile is ejected from a low position $\simeq 2\text{m}$ and at an initial climb close to 45° . Note also that the 270 ton counterweight falls only $\simeq 9\text{cm}$ ($\simeq 2L_2$).

The motion on the larger- l_4 branch is more complicated because the mass of the beam never ceases to matter ($\mu_b l$ rises with l). The final oscillations of beam and counterweight are in phase with frequency $\simeq \{g/(L_2 + L_3)\}^{1/2}$ as before, but with small internal oscillations of a similar frequency (more like a flexible body), and the transition to the oscillating mode is towards maximum amplitude where the counterweight comes to rest before the final oscillations start. This transition to harmonic motion is also much softer than the previous: The reaction force from the bearings rises only a little above Mg , and the sling tension stays below $20mg$. The configuration at release is again almost vertical, the projectile is ejected from a high position $\simeq 40\text{m}$ at a slightly smaller initial climb 42.6° , and the 71 ton counterweight now falls about $1/2\text{ m}$.

References

- [1] Hansen, P. V., *Acta Archaeologica*, **63**, (1992), pp189-268
- [2] Chevedden, P. E., Eigenbrod, L., Foley, V., and Soedel, W. (1995), *Sci. Am.* **273**, pp66-71.
- [3] Chevedden, P. E. (2000), *Dumbarton Oaks Papers*, 54. Washington D.C.
- [4] Fulton M. S., *Artillery in the Era of the Crusades: Siege Warfare and the Development of Trebuchet Technology*. History of Warfare, vol. 122, BRILL (2018).
- [5] Fulton M. S., Chrissis N. G., Phillips J. and Kedar B. Z. *Crusades*, (2017), **16**, pp33-53.
- [6] Galán M. R. and Galán M. B., *Archaeometry* 62, 5 (2020) 904–916
- [7] Saimre T., *Estonian Journal of Archaeology*, (2006), **10**, 1, pp61-80.
- [8] Denny M., 2005 *Eur. J. Phys.* 26 561
- [9] Goodno B. J. and Gere J. M. *Mechanics of materials*, 2009.
- [10] Facsimile of the Sketch-Book of Villars de Honnecourt, J. B. A. Lassus and J. Quicherat, trans. and ed. R. Willis (London, 1859);